Available online at www.sciencedirect.com
ScienceDirect
Physics Procedia 73 (2015) 59 – 66
Physics Procedia

4th International Conference Photonics and Information Optics, PhIO 2015, 28-30 January 2015

# Negative curvature hollow-core fibers: dispersion properties and femtosecond pulse delivery

A.N. Kolyadin[a]*, G.K. Alagashev[a], A.D. Pryamikov[a], L. Mouradian[b], A. Zeytunyan[b], H. Toneyan[b], A.F. Kosolapov[a], I.A. Bufetov[a]

[a]*Fiber Optics Research Center of Russian Academy of Sciences, Vavilova str. 38, Moscow, 119333, Russia*
[b]*Laboratory of Ultrafast Optics and Photonics, Faculty of Physics, Yerevan State University, 1 Alex Manoogian Street, Yerevan 0025, Armenia*

**Abstract**

In this work a comparative analysis of dispersion properties of hollow core photonic crystal fibers (HC PCFs) and negative curvature hollow core fibers (NCHCFs) was carried out. It was shown that the main reason for the low dispersion slope of NCHCFs is a strong light localization in the air core in comparison with HC PCFs. The strong light localization in NCHCFs allows not to use the complicated photonic crystal cladding and to reduce the air mode interaction with silica glass elements of the cladding. This conclusion was confirmed by experimental measurement of the group velocity dispersion and femtosecond pulse transmission for the NCHCF.

Peer-review under responsibility of the National Research Nuclear University MEPhI (Moscow Engineering Physics Institute)

*Keywords:hollow-core fibers; dispersion;laser pulse delivery.*

## 1. Introduction

Hollow-core microstructured optical fibers (HC MOFs) are waveguides which allow light to be localized and transmitted in the hollow core. The mechanisms of light localization in HC MOFs are different for different types of microstructured claddings. The light localization in HC MOFs with complicated cladding structure is achieved by constructive interference which occurs under light scattering from the 1D or 2D photonic crystal cladding. The spectral ranges where radiation cannot propagate in the radial direction are called photonic band gaps. The band edges are determined by the resonances or antiresonances in the individual elements of the cladding according to the ARROW (AntiResonant Reflecting Optical Waveguide) model (White et al. 2006).

For example, the mechanism of light localization in HC PCFs is based on the presence of photonic band gaps of a 2D photonic crystal in the cladding (Cregan 1999) (Fig. 1(1)). HC PCFs have the complex topological structure of the silica-air photonic crystal cladding and the photonic band gap is formed by three types of cladding two-dimensional resonators, namely, interstitial silica apexes, silica struts and air holes(F. Couny et al. 2007). The group velocity dispersion (GVD) of HC PCFs was investigated in works (Ziemienczuk et al. 2012; Matos & Taylor 2003; Ponzo et al. 2014). It was shown that the dispersion characteristics of HC PCF allow to compress laser pulses to sub - 100 – fs duration at 100 W average power (Rothhardt et al. 2011).

* Corresponding author Tel.:+7-499-503-81-93
*E-mail address:* kolyadin@fo.gpi.ru


Peer-review under responsibility of the National Research Nuclear University MEPhI (Moscow Engineering Physics Institute)
doi:10.1016/j.phpro.2015.09.122

Another type of HC MOFs with complicated cladding structure is hollow-core fibers with a Kagome lattice cladding (F Couny et al. 2007) (Fig. 1(2)). The mechanism of light localization in such HC MOFs is different from that for HC PCFs and in the literature this approach to the localization phenomenon is called the Inhibited coupling model (ICM) (F Couny et al. 2007).Comparatively small losses in such HC MOFs are caused by a strong transverse-field mismatch between the core and cladding modes (F Couny et al. 2007). The dispersion characteristics of hollow-core fibers with a Kagome lattice cladding were investigated in works (Wang et al. 2012; Mak et al. 2013; Debord et al. 2014). The authors of (Wang et al. 2011), (Wang et al. 2010) reported on the fabrication of the Kagome lattice HC PCF with a hypocycloid shaped core structure (Fig. 1(3)). They demonstrated starting from the inhibited coupling model that such design of core shape enhances the coupling inhibition between the core and cladding modes. In (Debord et al. 2014) the authors reported on the record transportation of mJ energy pulses of 600 fs duration operating around 1030 nm in the hypocycloid-core Kagome HC PCF.

In recent years, a new type of HC MOFs with a simple cladding consisting of only one layer of circular or elliptic cylinders (Kosolapov et al. 2011; Pryamikov et al. 2011) (Fig. 1(4,6)) (revolver fibers) or the stylized form of parachute(Yu et al. 2012)(Fig. 1(5)) (parachute fibers) have been proposed and extensively investigated.

All these fibers are characterized by the negative curvature of core-cladding boundary (Negative Curvature Hollow Core Fibers - NCHCFs).

It was demonstrated to be possible to guide light in revolver fibers made of silica glass up to a wavelength of 8 μm despite a comparatively simple construction of the non-photonic crystal cladding (Kolyadin et al. 2013). According to our estimations revolver fibers with one row of capillaries in the cladding provide the highest degree of light power localization in air - approximately 99.993% (Kosolapov et al. 2014). This fact shows that the physical mechanism of light localization in NCHCFs is different from those in other types of HC MOFs.

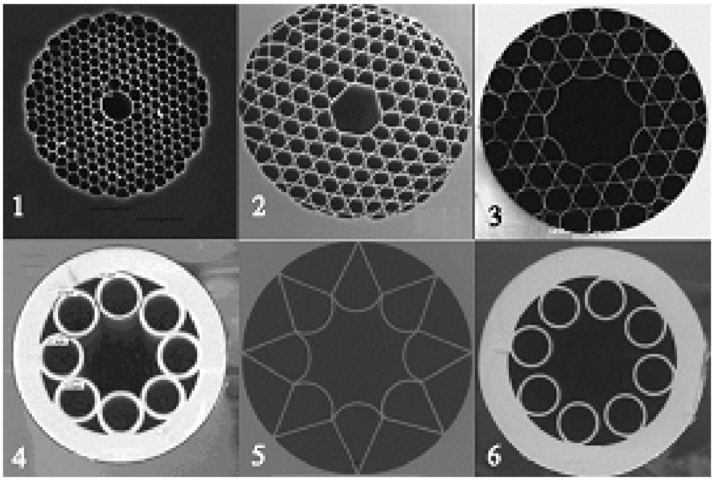


Fig. 1. SEM images of different types of hollow core fibers. 1- HC PCF (Benabid et al. 2004); 2- Kagome HC PCF (Benabid et al. 2002); 3- Kagome HC PCF with hypocycloid shaped core structure (Wang et al. 2011); 4- revolver NCHCF with connected capillaries (Pryamikov et al. 2011); 5- hollow-core fiber with elements which have stylized form of parachute (Yu et al. 2012); 6- revolver NCHCF with separated capillaries (Kolyadin et al. 2013).

Hollow-core fibers opened new opportunities in laser pulse compression and pulse transmission (Wang et al. 2012; Mak et al. 2013; Guichard et al. 2015). It is very important to know dispersion properties of hollow-core fibers for these applications. Up to this date, there was no information in the literature about group velocity dispersion in NCHCFs.

In this paper, we have carried out an analysis of dispersion properties of HC PCFs and NCHCFs to explain the low dispersion slopes occurring in all transmission bands in the latter case. All calculations were performed using commercial packet Femlab 3.1. The results of GVD measurements for real fibers are also presented. The GVD was measured for real revolver fiber and it was shown that the experimental results coincide very well with theoretical predictions. In addition, we demonstrated 748 nm laser pulse delivery in this fiber with pulse duration of several hundreds femtoseconds.

## 2. Analysis of differences between dispersion characteristics of HC PCF and NCHCF

To establish the reason of difference between the dispersion characteristics of HC PCF and NCHCF the difference between optical properties of the model waveguide structures shown in Fig. 2 (a, b) was numerically analyzed. It can be seen that the waveguide structures shown in Fig. 2(a) is a dielectric tube 1 made of silica glass suspended in air. It can be considered as HC PCF core-cladding boundary with continuous rotational symmetry (compare Fig. 1(1)). The dielectric tube has a core diameter of 78 μm and the wall thickness of 2.7 μm. The auxiliary cylinder 2 shows the region where the value of the field was set to zero (boundary condition).

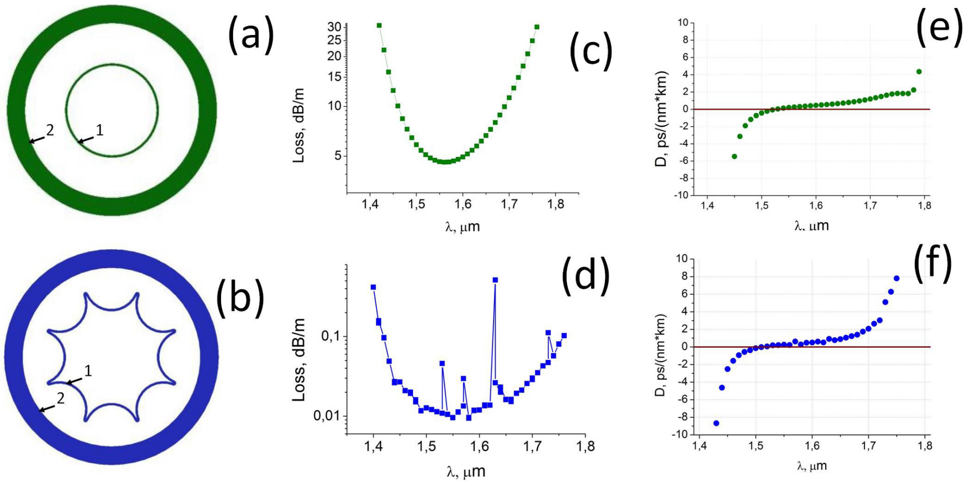


Fig. 2. (a) the HC PCF core-cladding boundary (1- glass capillary, 2- region of boundary condition 190μm diameter); (b) the NCHCF core-cladding boundary(1- glass capillary, 2- region of boundary condition 190μm diameter); (c) the waveguide loss for the structure show in Fig. 1(a); (d) the waveguide loss for the structure shown in Fig. 1(b); (e) the dispersion curve for the waveguide structure shown in Fig. 1(a); (f) the dispersion curve for the waveguide structure shown in Fig. 1(b).

The second structure that was analyzed is shown in Fig. 2b. The main part of it is a dielectric tube 1 with negative curvature boundary made of silica glass. The wall thicknesses and effective area of the air core modes are the same as in the case of the dielectric tube (Fig. 2(a)). It is clear that only two factors strongly affect on the waveguide properties of real HC PCFs and NCHCFs, namely, the shape of the core cladding boundary and the microstructured cladding. Model waveguide structures shown in Fig. 2a, b may be considered as hollow core fibers without any microstructured cladding. In order to appreciate the physical mechanism responsible for formation of dispersion slope in the case of HC PCF and NCHCF the waveguide loss and dispersion curves for the model waveguide structures (Fig. 2 a, b) were calculated .The results obtained are shown in Fig. 2c, d. As one can see, the waveguide loss of the dielectric tube (Fig. 2(a)) differs from the one of the negative curvature tube (Fig. 2(b)) by several orders. Several resonances in the transmission band Fig. 2(d) occur due to an excitation of collective electromagnetic states of the negative curvature boundary and their coupling with the air core modes. This mechanism of the collective states excitation was described in(Alagashev et al. 2015). The stronger light localization in the air core of the tube with negative curvature boundary occurs due to different mechanism of light localization in different parts of the negative curvature boundary (including the ARROW mechanism). To obtain the same level of the waveguide loss for the dielectric tube (Fig. 2(a)) it is necessary to add the photonic crystal cladding with several layers of microstructured elements to the tube. Based on the loss level (Fig. 2(c, d)) it is possible to state that the air core modes leaking out of the tube (Fig. 2(a)) have to interact much more strongly with the photonic crystal cladding in comparison with the air core modes of the negative curvature tube (Fig.2 (b)).

The dispersion curves for the waveguide structures (Fig. 2 (a, b)) are shown in Fig. 2(e, f). As one can see from Fig. 2(e, f), the values of GVD of the tubes are very close to each other in the considered transmission band and the dispersion slopes are very small in both cases (~0.01 ps/nm$^2$*km). It is known that in real HC PCFs the dispersion slopes are much higher than in Fig. 2(e, f) (~29 ps/nm$^2$*km (Matos & Taylor 2003) and ~1.4 ps/nm$^2$*km Ponzo et al. 2014)). As it was discussed above, such increase of the dispersion slope occurs due to addition of complicated microstructured cladding to the dielectric tube (Fig. 2(a)) when the air core modes begin to interact with the glass elements of the bulk microstructured cladding. Consequently, the light localization mechanism of the tube shown in Fig. 2(b) allows not to add a complicated microstructured cladding to the core boundary and to keep the low dispersion slopes in all transmission bands. In the next Sections we will demonstrate this fact experimentally.

## 3. Experimental GVD measurement

We carried out experimental measurement of group velocity dispersion in the real hollow-core fiber (Fig. 4(a)).

The setup for the dispersion measurement (Fig. 3) uses a supercontinuum (SC) source and monochromator. Input fiber was used to deliver light in single mode from monochromator to a Mach-Zehnder interferometer. After input fiber beam goes to the interferometer: beam separates on a beam splitter, goes to reference arm or to arm with the fiber under test, converge on the second splitter and then incident on the CCD camera or germanium detector where we observed its interference. CCD camera was used to make sure that both beams are coaxial and interfere properly. The length of the reference arm could be changed by moving the prism: within wide range by micrometer screw and within narrow range by magnetic coil. Fiber SEM image and dispersion profile are shown in Fig.4.

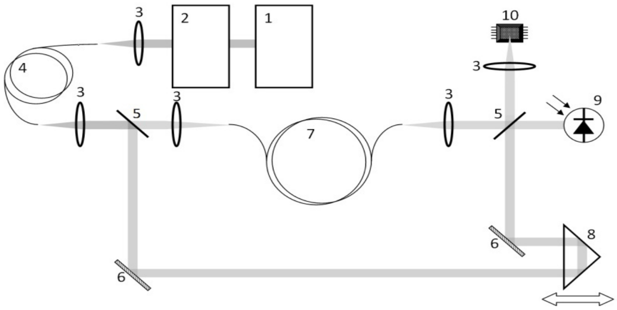


Fig. 3. Schematic of the experimental setup. 1- supercontinuum source, 2- monochromator, 3- microscope objectives, 4- input fiber, 5- beam splitters, 6- mirrors, 7- hollow-core fiber under test, 8- prism on electromechanical suspension, 9- germanium detector, 10- CCD camera.

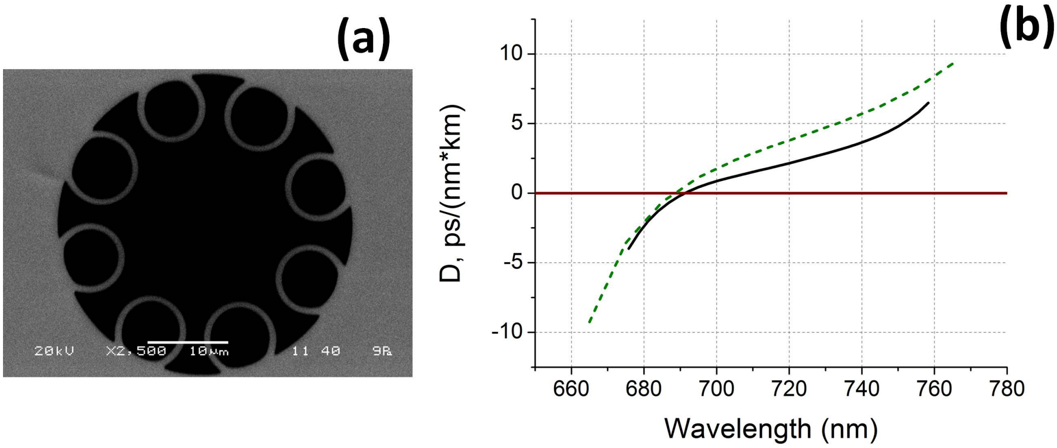


Fig. 4 (a) NCHCF SEM image and (b) measured (solid black) and computed (dashed green) GVD of the fiber.

Fiber used in the experiment has 21μm core diameter (inscribed circle), capillaries around the core have 828 nm wall thickness. In experiment we used fiber 8.6 m long. With fiber length shorter than two meters mode content wasn't stable during wavelength scanning. So we increased the length to achieve single mode distribution regime (we had similar problems in (Kolyadin et al. 2013)). Mode content was analyzed in the far field by the CCD camera. The data obtained in the experiment were approximated by the $6^{th}$ degree polynomial with consequent differentiation.

To confirm our experimental results we also calculated dispersion in the model of the fiber used in the experiment. Calculated dispersion with the measured one are depicted in Fig.4(b) (dashed green and solid black curves correspondently). We conclude from Fig.4(b) that our computational and experimental data are in good agreement. Small deviations, in our opinion, are caused by difference in geometry between the model and the real fiber. In real fiber capillaries are not perfectly round (Fig. 4(a)), capillaries' wall thickness slightly vary in each capillary and from one to one (which wasn't taken into account in the model).

## 4. Femtosecond pulse delivery

To study the dispersion characteristics of the fiber shown in Fig.4a by another method, we carried out spectral and autocorrelation measurements of femtosecond pulses at the input and output of the fiber. The measurements were fulfilled in 2 regimes of femtosecond laser operation (FWHM pulse duration $\tau \approx 180$ fs (255 fs autocorrelation duration) that corresponds to ~4-nm bandwidth, and $\tau \approx 125$ fs (180 fs autocorrelation duration) with ~7-nm bandwidth). We used a 20x (0.4 NA) microscope objective to couple the beam from the Coherent Verdi V10 + Mira 900F femtosecond laser system with the following parameters of radiation: >1 W average power at a 76 MHz repetition rate, 748 nm central wavelength. We also added different blocks of SF11 glass to compress the pulses at the fiber output and with this to make sure that the fiber gives anomalous dispersion. The length of the fiber was 10 m in most experiments.

*4.1. Transmission of 255 fs pulses*

In this regime, the average power of the laser radiation was 1.3 W, and the average power at the fiber output was ~100 mW. Fig.5 shows the spectra (i, iii, v) and autocorrelation traces (ii, iv, vi) of the pulses at the fiber input (Fig.5 (i, ii)), at the fiber output (Fig.5 (iii, iv)), and at the fiber output when a 10-cm block of SF11 glass was added before (Fig.5 (v; vi, line 1)) and after (Fig.5(vi, line 2) the fiber. Lines 1 and 2 are very close to each other. After propagating through the fiber, the spectrum remains almost constant, and the duration of the autocorrelation trace increases from 255 fs to 514 fs (FWHM). The measured autocorrelation trace at the fiber input has 255 fs duration (line 1 in Fig.5(ii)), and the calculated Fourier-transform pulse of the measured spectrum has 236 fs autocorrelation duration (line 2 in Fig.5(ii)). This means that the laser gives slightly positively chirped pulses, with the amount of group delay dispersion (GDD) equal to +3,500 fs$^2$. Thus, during the pulse propagation in the fiber, first takes place pulse compression due to the fiber anomalous dispersion, and after that takes place pulse dispersive stretching. We add GDD = –22,900 fs$^2$ on top of the spectrum to obtain the measured autocorrelation duration of 514 fs at the fiber output. Note that GDD = $\beta_2 z$ , where $z$ = 10 m is the fiber length and $\beta_2$ is the second-order dispersion coefficient. Hence, we find $\beta_2$ = –2,290 fs$^2$/m (D=7,7 ps/(nm*km)). Adding a 10-cm block of SF11 glass allows to compress the pulses stretched in the fiber down to 280 fs autocorrelation duration, proving that the pulse stretching takes place due to the anomalous dispersion of the fiber. Moreover, SF11 glasses added before and after the fiber give roughly the same autocorrelation traces for the compressed pulse (lines 1 and 2 in Fig.5(vi)). Together with the fact that the spectrum does not change after the fiber, this allows to assume that there is no nonlinearity in the fiber. However, the durations of the initial and compressed pulses do not match, which presumably means that the induced chirp is not purely linear. The slight difference of the measured and calculated autocorrelation traces at the fiber output (lines 1 and 2 in Fig.5(iv), respectively) also points out the presence of high-order dispersion.

We can estimate the value of $\beta_2$ by another rough method. For the propagation of transform-limited Gaussian pulses in a dispersive medium, we have $(\tau/\tau_0)^2 = 1 + (z/L_d)^2$ , where $\tau_0$ is the initial pulse duration (half-width at $e^{-1}$ level), $\tau$ is the chirped pulse duration, and $L_D = (\beta_2 \Delta\omega_0^2)^{-1}$ is the dispersive length with the initial pulse bandwidth $\Delta\omega_0 = 1/\tau_0$ . Further, $\beta_2$ can be calculated from this formula: $\beta_2 = [(\tau/\tau_0)^2 - 1]^{1/2} / [z\Delta\omega_0^2]$ . In this regime, we got the value $\beta_2$ = –2,390 fs$^2$/m, which is in a good agreement with the pure experimental measurement $\beta_2$ = –2,290 fs$^2$/m without any assumptions for the pulse shape and chirp.

*4.2. Transmission of 180 fs pulses*

In this regime, the average power of the laser radiation was 1.1 W, and the average power at the fiber output was ~90 mW. Again, Fig.6 shows the spectra (i, iii, v) and autocorrelation traces (ii, iv, vi) of the pulses at the fiber input (Fig.6 (i, ii)), at the fiber output (Fig.6 (iii, iv)), and at the fiber output when a 10-cm block of SF11 glass was also added before (Fig.6 (v; vi, line 1)) and after (Fig.6 (v; vi, line 2) the fiber. After propagating through the fiber, the spectral bandwidth decreases from ~6.4 nm to ~5.7 nm, meaning that the fiber slightly cuts the spectrum. This can be understood taking into account the losses curve of the fiber. The duration of the autocorrelation trace increases from 180 fs to 592 fs. The measured autocorrelation trace at the fiber input has 180 fs duration, and the calculated Fourier-transform pulse of the measured spectrum has 169-fs autocorrelation duration. This means that the laser gives slightly positively chirped pulses, with the amount of GDD equal to +2,100 fs$^2$. In this case we add GDD = –19,250 fs$^2$ on top of the spectrum to obtain the measured autocorrelation duration of 514 fs at the fiber output. Hence, we find $\beta_2$ = –1,925 fs$^2$/m (D=6,5 ps/(nm*km)). Adding a 10-cm block of SF11 glass before and after the fiber allows to compress the pulses stretched in the fiber down to 207 fs autocorrelation duration. In this regime, the durations of the initial and compressed pulses also do not match, and again there is a slight difference between the measured and calculated autocorrelation traces at the fiber output (lines 1 and 2 in Fig.6(iv), respectively). According to the rough estimation method, in this regime for the second-order dispersion coefficient we got the value $\beta_2$ = –1,850 fs$^2$/m.

*4.3. Transmission through 1m fiber*

We carried out the same set of experiments for a 1-m long fiber. In this case we had higher average powers at the fiber output: ~370 mW in the regime of ~4-nm bandwidth pulses, and ~300 mW in the regime of ~7-nm bandwidth pulses. There was no significant pulse stretching in this case: 246 fs autocorrelation duration from 240 fs in the regime of ~4-nm bandwidth pulses, and 175 fs autocorrelation duration from 171 fs in the regime of ~7-nm bandwidth pulses. More interestingly, in this regime we observed spectral beatings at the fiber output (Fig.7(i)). This is presumably due to the interference between the fiber modes (the final mode is not shaped in case of short fiber). The figure below shows the measured spectrum (Fig.7(i)), and the measured autocorrelation trace (Fig.7(ii, line 1)) in comparison with the calculated Fourier transform (Fig.7(ii, line 2)) of the spectrum.

To conclude, we obtained the values $\beta_2$ = –2,290 fs$^2$/m (D=7,7 ps/(nm*km)) and $\beta_2$ = –1,925 fs$^2$/m (D=6.5 ps/(nm*km)) for two different regimes of our experiments. The difference between these results can be understood taking into account higher order dispersion of the fiber. The results obtained are in a good agreement with results of Section 3.

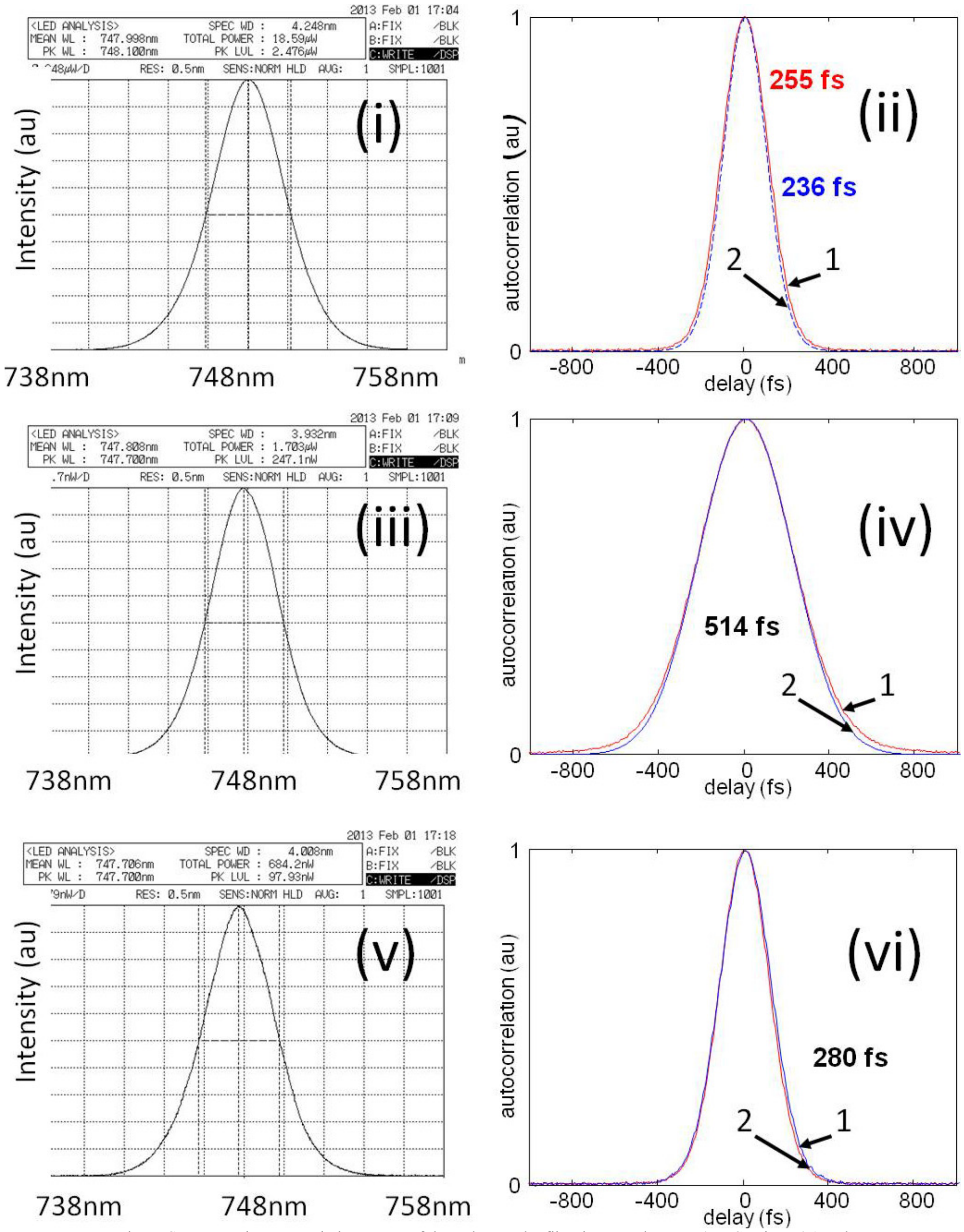


Fig. 5. Spectra and autocorrelation traces of the pulses at the fiber input and output (see Sections 4.1 and

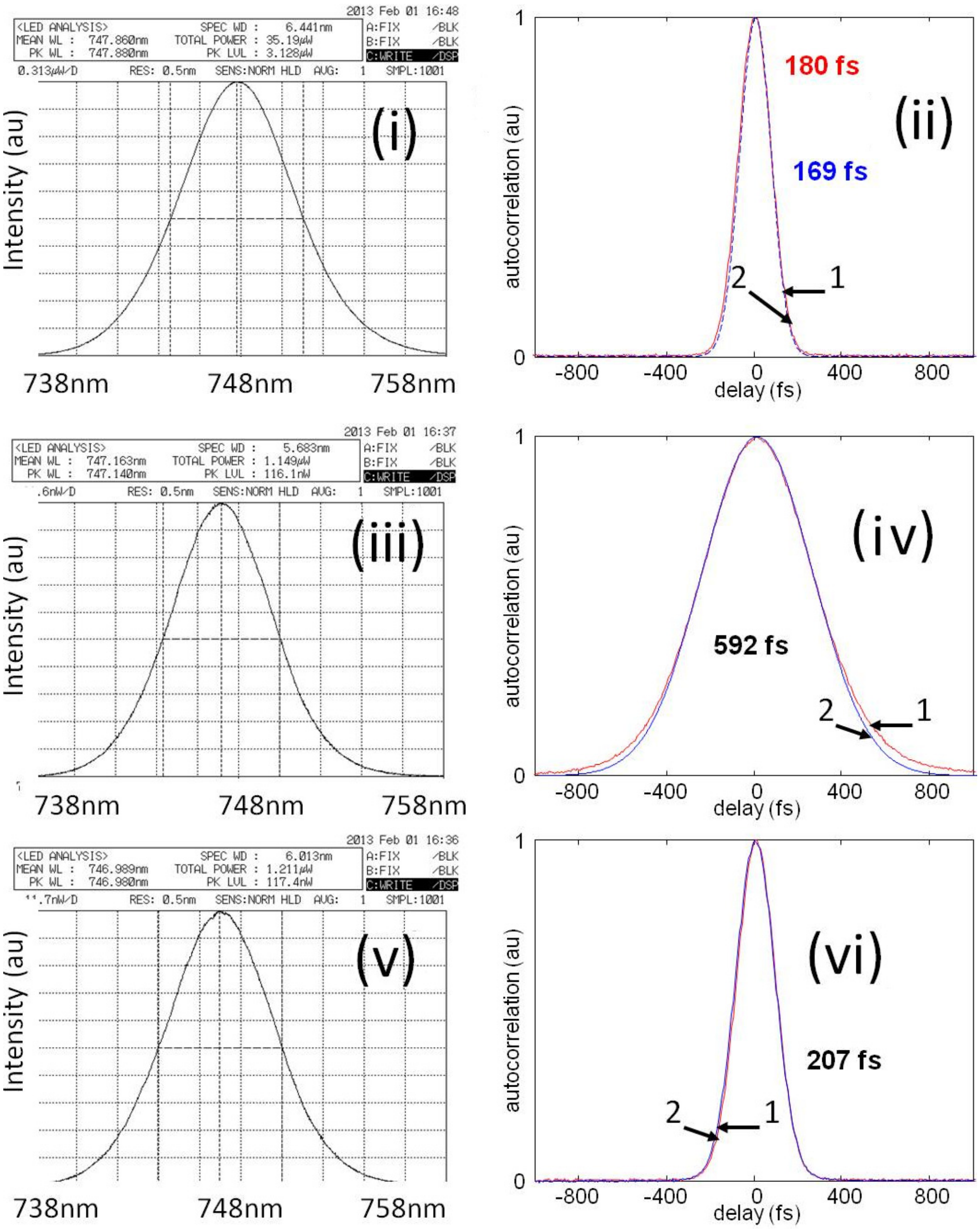


4.2).

Fig. 6. Spectra and autocorrelation traces of the pulses at the fiber input and output (see Sections 4.1 and 4.2).

## 5. Conclusions

It is shown that the dispersion slope of model of thin wall capillary fibers (Fig. 2a,b) is determined mainly by the thickness of the wall and depends only slightly on the shape of the capillary cross section. The addition of the complicated photonic crystal cladding results in an essential increase of waveguide dispersion slope. For this reason NCHCFs (both revolver fibers and parachute fibers, all without photonic crystal cladding) show essentially lower dispersion in comparison with hollow core PCFs and are promising for femtosecond pulses delivery in technological arrangements.

Experimental data of dispersion in NCHCF (in revolver fibers) are presented for the first time. The delivery of femtosecond laser pulses with broadening from 255 to 514 fs autocorrelation duration at wavelength of 748 nm and with 1 W average power at 76 MHz repetition rate was demonstrated for the revolver 10 m long fiber. Fiber of the same type but only 1 m long can deliver 180 fs laser pulses without broadening. This is a direct demonstration of possibilities of hollow core revolver fibers to deliver femtosecond laser pulses without distortion for technological purposes.

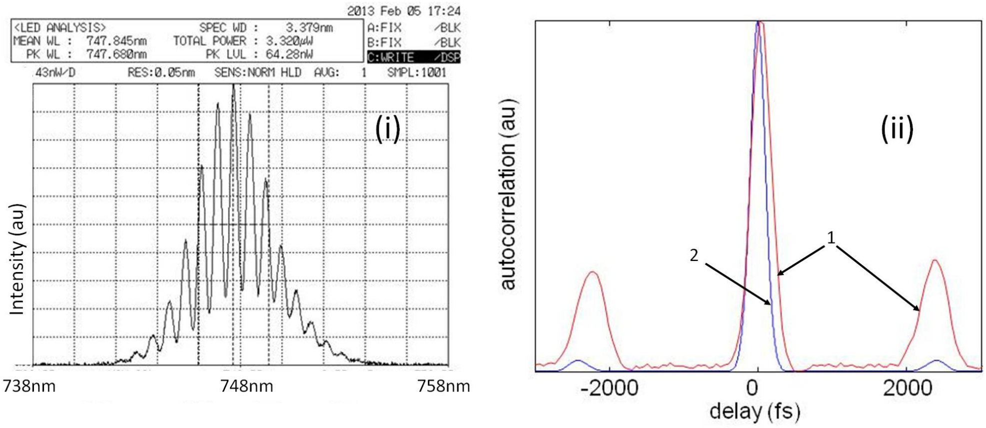


Fig. 7. Spectrum and autocorrelation traces (see Section 4.3).

**Acknowledgements**

This work was supported by the Russian Foundation for Basic Research, grant #14-29-07176-ofi_m.

**References**

Alagashev, G.K. et al., 2015. Impact of geometrical parameters on the optical properties of negative curvature hollow-core fibers. Laser Physics 25(5), 055101.
Benabid, F. et al., 2002. Stimulated Raman scattering in hydrogen-filled hollow-core photonic crystal fiber. Science (New York, N.Y.), 298(5592), 399–402.
Benabid, F. et al., 2004. Ultrahigh Efficiency Laser Wavelength Conversion in a Gas-Filled Hollow Core Photonic Crystal Fiber by Pure Stimulated Rotational Raman Scattering in Molecular Hydrogen. Physical Review Letters 93(12), 123903.
Couny, F. et al., 2007. Generation and photonic guidance of multi-octave optical-frequency combs. Science (New York, N.Y.), 318 (5853), 1118–21.
Couny, F. et al., 2007. Identification of Bloch-modes in hollow-core photonic crystal fiber cladding. Optics Express 15(2), 325.
Cregan, R.F., 1999. Single-Mode Photonic Band Gap Guidance of Light in Air. Science 285(5433), 1537–1539.
Debord, B. et al., 2014. Multi-meter fiber-delivery and pulse self-compression of milli-Joule femtosecond laser and fiber-aided laser-micromachining. Optics express 22(9), 10735–46.
Guichard, F. et al., 2015. Nonlinear compression of high energy fiber amplifier pulses in air-filled hypocycloid-core Kagome fiber. Optics Express 23(6), 3866–3869.
Kolyadin, A.N. et al., 2013. Light transmission in negative curvature hollow core fiber in extremely high material loss region. Optics express 21(8), 9514–9.
Kosolapov, A.F. et al., 2011. Demonstration of CO 2 -laser power delivery through chalcogenide-glass fiber with negative-curvature hollow core. Optics express 19(25), 9–14.
Kosolapov, A.F. et al., 2014. Negative Curvature Hollow-Core Fibers (NCHCFs) for Mid-IR Applications. Advanced Photonics OSA Technical Digest (online) (Optical Society of America, 2014), paper, p.SoTu2B.3.
Mak, K.F. et al., 2013. Two techniques for temporal pulse compression in gas-filled hollow-core kagomé photonic crystal fiber. Optics letters 38(18), 3592–5.
Matos, C.J.S. De & Taylor, J.R., 2003. All-fiber chirped pulse amplification using highly-dispersive air-core photonic bandgap fiber. Optics Express 11(22), pp.1702–1704.
Ponzo, G.M. et al., 2014. Fast and broadband fiber dispersion measurement with dense wavelength sampling. Optics express, 22(1), pp.943–53.
Pryamikov, A.D. et al., 2011. Demonstration of a waveguide regime for a silica hollow--core microstructured optical fiber with a negative curvature of the core boundary in the spectral region > 3.5 μm. Optics express, 19(2), pp.1441–1448.
Rothhardt, J. et al., 2011. 1 MHz repetition rate hollow fiber pulse compression to sub-100-fs duration at 100 W average power. Optics Letters 36(23), 4605.
Wang, Y.Y. et al., 2012. Design and fabrication of hollow-core photonic crystal fibers for high-power ultrashort pulse transportation and pulse compression. Optics letters 37(15), 3111–3113.
Wang, Y.Y. et al., 2011. Low loss broadband transmission in hypocycloid-core Kagome hollow-core photonic crystal fiber. Optics letters 36(5), 669–671.
Wang, Y.Y. et al., 2010. Low loss broadband transmission in optimized core-shape Kagome Hollow-Core PCF. Lasers and Electro-Optics (CLEO) and Quantum Electronics and Laser Science Conference (QELS), 2010 Conference on (2010), p.CPDB4.
White, T.P., Mcphedran, R.C. & Sterke, C.M. De, 2006. Resonance and scattering in microstructured optical fibers. Optics Express 27(22), 1977–1979.
Yu, F., Wadsworth, W.J. & Knight, J.C., 2012. Low loss silica hollow core fibers for 3 – 4 μ m spectral region. Optics Express 20(10), 11153–11158.
Ziemienczuk, M. et al., 2012. Intermodal stimulated Raman scattering in crystal fiber. J. Opt. Soc. Am. B 29(7), 1563–1568.